Effect of the addition of Si into Nb$_2$O$_5$ coatings on their structural, optical, and mechanical properties

Roberto Mirabal-Rojas Stephen Muhl and Sandra E. Rodil Enrique Camps Michael Lejeune and Andreas Zeinert

Effect of the addition of Si into Nb_2O_5 coatings on their structural, optical, and mechanical properties

Roberto Mirabal-Rojas
Instituto de Investigaciones en Materiales, Universidad Nacional Autónoma de México, Circuito Exterior s/n CU, México D.F. 04510, Mexico and Posgrado en Ciencia e Ingeniería de Materiales, Universidad Nacional Autónoma de México, Unidad de Posgrado, Edificio C, Piso 1, Zona Cultural de CU, México D.F. 04510, Mexico

Stephen Muhl and Sandra E. Rodil[a]
Instituto de Investigaciones en Materiales, Universidad nacional Autónoma de México, Circuito Exterior s/n CU, México D.F. 04510, Mexico

Enrique Camps
Instituto Nacional de Investigaciones Nucleares, Carretera México-Toluca S/N, kilómetro 36.5. La Marquesa, Municipio de Ocoyoacac, CP 52750 Estado de México, Mexico

Michael Lejeune and Andreas Zeinert
Laboratoire de Physique de la Matière Condensée, Université de Picardie Jules Verne, 33 rue Saint Leu, 80039 Amiens Cedex 1, France

There are many polymorphs of Nb_2O_5, each with interesting properties that have been explored for biomedical, photocatalytic, and optical applications. However, Nb_2O_5 is not generally used for mechanical applications owing to its low hardness (8 GPa). The objective of this work was to evaluate the effects resulting from the addition of silicon (Si) into the Nb_2O_5 structure, with the aim of increasing its hardness through the formation of a nanostructured composite coating. In this paper, the authors report the structure and mechanical properties of Nb_2O_5 as a function of the silicon content (0–5.5 at. %). The coatings were deposited on silicon and D2 steel substrates using a confocal-dual magnetron sputtering system using a mixture of argon and oxygen (80:20) with each magnetron (Nb and Si targets) independently driven. The coatings were annealed at 550 °C to obtain a crystalline structure. However, analysis of the optical properties indicated the persistence of a substoichiometric amorphous phase. Despite the contribution of the amorphous phase, the mechanical–tribological properties were slightly improved after Si incorporation. The hardness reached a maximum of 17.6 GPa for the samples deposited at 50 W in the Si target, coupled with a reduction in both the coefficients of friction and wear. © *2016 American Vacuum Society*.
[http://dx.doi.org/10.1116/1.4954985]

I. INTRODUCTION

Niobium oxide coatings have been studied for various applications, many of which take advantage of their optical properties including a high refractive index (above 2.1 at 500 nm) and wide band gap.[1–3] Some examples include catalytic photoactivated processes,[4–6] including photovoltaics,[7,8] water splitting,[9] and as an electrochromic material.[4,10–12] The dielectric properties of the niobium oxide coatings are also of interest for capacitors,[13–16] sensors,[17,18] and memory devices.[19] There are also some reports of biomedical applications of these coatings owing to their high chemical and corrosion resistance.[20–23] However, much less is known about the mechanical properties of the Nb_2O_5 coatings. The hardness of sputtered deposited amorphous Nb_2O_5 coatings has been reported by Ramirez *et al.*[24] and Mazur *et al.*[2] showing that the hardness depends upon the deposition conditions and varies between 3.9 and 5.6 GPa. Meanwhile, Çetinörgü-Goldenberg *et al.*[25] have reported the hardness and elastic modulus of the T-Nb_2O_5 phase with values of 6.8 and 132 GPa, respectively. Niobium oxides form a family of materials presenting different compositions, structures, and properties.[14,26] The basic phase diagram identifies three different compositions of NbO, NbO_2, and Nb_2O_5 whose electronic character changes from metallic to a small band-gap semiconductor and finally to an insulating or large band-gap semiconductor, respectively.[14] However, solid solutions and nonstoichiometric phases have also been reported.[27–29] As a coating, the most commonly reported composition is niobium pentoxide or niobia (Nb_2O_5), which has different polymorphic forms[14,30] and has interesting optical properties. These properties include a band gap above 3 eV and a high refractive index, making it suitable for a wide range of optical applications. Among these different polymorphs, the most frequently produced are the pseudohexagonal TT-Nb_2O_5, obtained between 400 and 500 °C; the orthorhombic T-Nb_2O_5, obtained between 500 and 600 °C; and the monoclinic H-Nb_2O_5, obtained above 1000 °C, while below 400 °C the Nb_2O_5 is usually amorphous.[6,12,24,26,31–33]

A wide range of deposition or synthesis methods for Nb_2O_5 coatings have been used, including anodization,[34–37] sol–gel,[10,38–40] spray pyrolysis,[40,41] vapor deposition,[42–44] and sputtering.[2,24,45–48]

[a]Electronic mail: srodil@unam.mx

Because the hardness values of the Nb$_2$O$_5$ coatings are relatively low (<6 GPa), Nb$_2$O$_5$ coatings are not considered suitable for mechanical applications such as machining or forming tools. However, if the hardness could be increased well above that of glass (Corning Gorilla® glass; 5.5–6.5 GPa), then the optical properties of the Nb$_2$O$_5$ material in combination with its corrosion[23,24] and thermal oxidation resistance[49] may be a benefit for some applications such as solar cells, optical sensors, capacitors, and memories.

The objective of this work was to evaluate the effect of the addition of silicon (Si) into polycrystalline niobium oxide coatings with the aim of increasing the hardness of the material through the formation of a nanostructured composite coating. Such an approach has been previously used to improve the hardness of metal nitride coatings[50–54] by adding an amorphous SiN$_x$ secondary phase. The nanocomposite hardening effect works because of the synergy between the dislocation-free metal nitride nanocrystals and impairment of the dislocation movement through the amorphous matrix even under high-applied stress. The addition of Si between 7 and 11 at. % leads to a substantial increase in the hardness from that of metal nitride (about 25 GPa) to 40–60 GPa for TiN:Si (Ref. [50]) or to 38 GPa for NbN:Si.[55] Other authors have also reported that the addition of Si into metal nitride coatings leads to hardness enhancement but through mechanisms such as solid solution hardening or defects.[56,57] However, the use of Si addition as a mechanism to augment the mechanical strength of oxide coatings has not been explored carefully. Voevodin *et al.*[58] have obtained AlSiO$_x$ coatings deposited by the electrochemical oxidation of Al alloys with a high voltage spark treatment in an electrolyte bath containing NaSiO$_3$, so that SiOx was incorporated into the Al$_2$O$_3$ coating. They reported the synthesis of a composite coating consisting of a hard (18–25 GPa) Al$_2$O$_3$ phase and a softer (2 GPa) alumina-silicate phase. However, the presence of the soft phase leads to degradation of the mechano-tribological properties. Nb-Si composite coatings[59] have been prepared for solar-absorption coatings, and Nb$_2$O$_5$-SiO$_2$ multilayers[60] have been proposed to control the stress in optical coatings for applications in micromechanical systems or as a reflection layer in optical lenses.[61]

The present paper reports screening experiments to determine the effect of the addition of Si into niobium oxide coatings deposited via reactive magnetron sputtering using two independent targets (Nb and Si). The variations in the structure, morphology, optical, and mechanical–tribological properties are reported as a function of the power applied to the Si target.

II. EXPERIMENTAL PROCEDURES

A. Deposition conditions

The Nb-O system includes NbO, NbO$_2$, Nb$_2$O$_5$, and nonstoichiometric phases. Initial experiments were done to determine the deposition conditions that allow the production of coatings with a predominant T-Nb$_2$O$_5$ structure, as shown by x-ray diffraction (XRD) patterns. For this, the O$_2$ gas flow rate was changed from 2 to 8 standard centimeter

cubic meters (sccm) with a 2 sccm step size, while the Ar flow rate was fixed at 24 sccm. The working pressure was manually adjusted to 0.4 Pa, while the substrate temperature was varied between room temperature (RT), i.e., no external heating and 300 °C. Two separate power values (direct current) were applied to the Nb target of 200 and 400 W. From these screening experiments, we selected the following deposition conditions: an Ar/O$_2$ flow rate ratio of 24/6, 400 W applied to the Nb target, and no external heating applied to the substrate. This last condition was adapted because the coatings were amorphous for any of the tested temperatures, which made it important therefore to carry out annealing of the coatings after the deposition. The coatings were annealed in air at 550 °C for 2 h, whereupon, as shown later in the results, though XRD indicated a pure T-Nb$_2$O$_5$ phase, optical analysis revealed that the coatings contained a certain fraction of amorphous substoichiometric phases. Therefore, we will designate the coatings NbO$_x$.

The NbO$_x$:Si coatings were deposited on silicon (100), glass, and polished D2 steel disks. A confocal magnetron sputtering system was used in which the magnetrons (10 cm diameter) were positioned with their axes about 53° off the vertical, and the substrate–target distance was fixed at 100 mm. The substrates were mounted on a rotary sample holder [speed of 15 revolutions per minute (rpm)] to assure film homogeneity. The targets used were Nb (99.95% purity) and Si (99.999% purity) and were individually driven. The base pressure of the vacuum system was <4 × 10^{-4} Pa.

To deposit the NbO$_x$:Si coatings, the conditions described above were used, and the Si was added by increasing the radio frequency (rf) power applied to the Si target from 12 to 200 W. The plasmas were operated at the same time, but, in the case of the D2 steel substrates, a 300 nm Nb bonding layer was grown using only Ar (10 min). Subsequently, the O$_2$ was added, and the power to the Si target was applied.

The deposition time was fixed to allow determination of the effect of the power applied to the Si target, and therefore the amount of Si incorporation, upon the deposition rate. For the samples deposited on Si and glass, the deposition time was set at 45 min, and for the D2 steel substrates, the deposition time was fixed at 90 min (plus the 10 min for the Nb bonding layer).

B. Coatings characterization

The thickness of the coatings was evaluated using a Veeco Dektak 150 profilometer measuring the height of a step to a small uncoated area. The structural characterization was done on both the Si and D2 steel substrates using a Rigaku Ultima IV diffractometer (CuKα 1.5406 Å) in the Bragg Brentano scan configuration and the $\theta-2\theta$ mode from 15° to 60°; and by micro-Raman spectroscopy with a Horiba T64000 with a INNOVA 70C spectrum laser with a wavelength of 514 nm. The surface morphology and the composition of the coatings were obtained using a JEOL7600F field emission-scanning electron microscope with 10 kV of acceleration voltage, and with a coupled Oxford INCAX-ACT energy dispersive x-ray spectrometer (EDS). To study the

optical properties, a spectroscopic ellipsometry (samples deposited on Si) was used via a Jobin-Yvon UVISEL phase modulated ellipsometer in the 1.5–5 eV range and an energy step of 0.15 eV and an incidence angle of 70°.

The mechanical–tribological properties were measured on the coatings deposited on the D2 substrates. The hardness and elastic modulus of the coatings were evaluated by nano-indentation using a continuous stiffness measurement nano-indentator (model TTX) with a Berkovich-type pyramidal diamond tip. For each sample, six measurements were carried out, and the maximum load was chosen whereupon the penetration depth was <10% of the coating thickness.[62] The load range was between 1 and 3 mN, and the hardness was calculated using the Oliver–Pharr model.[63] The scratch test[64] was used to measure the adhesion between the coating and the steel substrate, and was performed using a TriboTechnic Millenium 100 instrument with a 6 mm steel pin and a variable load from 0 to 80 applied along an 8.5 mm distance at a displacement velocity of 8 mm/min. For each sample, three scratch test scans were carried out. The coefficient of friction (CoF) was measured using a TriboTechnic pin-on-disk tribometer with 6 mm Al$_2$O$_3$ balls, 1 N load at a linear speed of 0.5 m/s, and 500 m of sliding distance at RT. For each sample, the CoF was measured on three different samples to verify the reproducibility of the test. The wear tracks left by the pin-on-disk tests were subsequently observed by optical microscope, and the volume loss was estimated by measuring the depth of the wear-track using a stylus profilometer.

III. RESULTS AND DISCUSSION

A. Structure

Figure 1 shows the *in situ* XRD analysis of the initial T-Nb$_2$O$_5$ samples as a function of the annealing temperature, where it can be observed that the films are amorphous until the annealing temperature reaches 500 °C. At this temperature, the T-Nb$_2$O$_5$ orthorhombic phase (ICDD-01-071-0336) can be clearly identified and it does not change as the temperature increases up to 700 °C or after the sample is returned to RT. Similar behavior is observed as the Si content is increased, and therefore, all samples were annealed at 550 °C for 2 h. It is important to remark that no other Nb-O phases are observed by XRD. However, it is essential to mention that the low optical transmittance in the visible range of the samples suggests the presence of niobium oxide phases with lower oxygen content. These probably occupy a phase between NbO or NbO$_2$ in small quantities or are amorphous, as shown later.

Figure 2 shows the thickness of the coatings versus the power applied to the Si target for samples deposited on Si (45 min) and D2 steel (90 min). It can be seen that, as the power applied to the Si target increases from 0 to 200 W, the thickness of the films doubles. Nevertheless, the Si incorporation into the films is relatively low, as can be observed also in Table I; so most probably, the increase in the deposition rate is a consequence of the densification of the plasma owing to the action of both magnetrons. Hereafter, the NbO$_x$:Si samples will be designated as NbO$_x$-P$_{Si}$, where P$_{Si}$
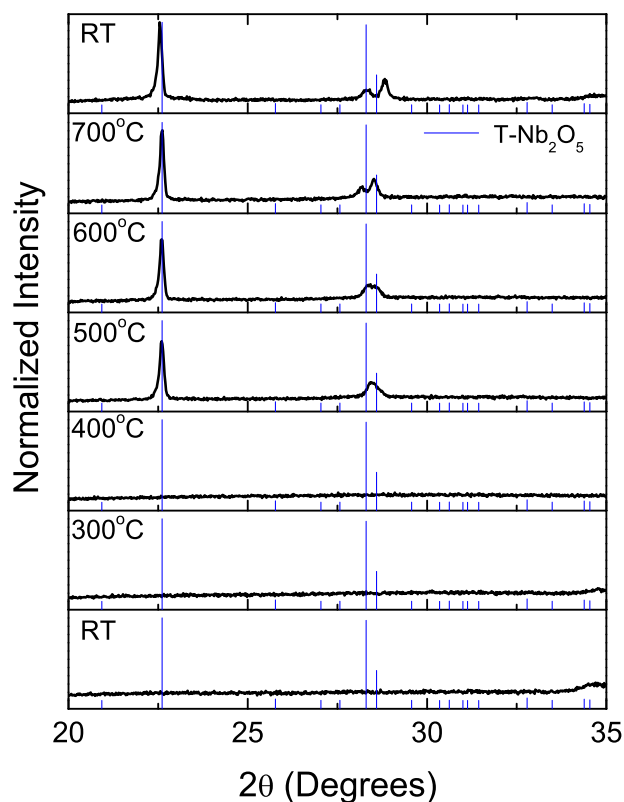

FIG. 1. (Color online) *In situ* XRD vs temperature (RT to 700 °C) analysis of the as-deposited niobium oxide coatings. Above 500 °C, the diffraction peaks can be assigned to the orthorhombic T-Nb$_2$O$_5$ phase (JCDPS card No. 01-071-0336). After cooling (pattern at top), the T-Nb$_2$O$_5$ phase is retained.

is the rf power applied to the Si target; and where the corresponding deposition conditions and Si at. % determined by EDS are indicated in Table I. The O/Nb ratio measured from the EDS analysis is also included in Table I, where it can be observed that, within the accuracy of the technique, the NbO$_x$ samples (no Si) has a ratio very close to the stoichiometric Nb$_2$O$_5$ composition. However, as the Si at. % is increased, the increase in O/Nb suggests an oxygen-rich niobium oxide, but it is more probably indicating that oxygen is
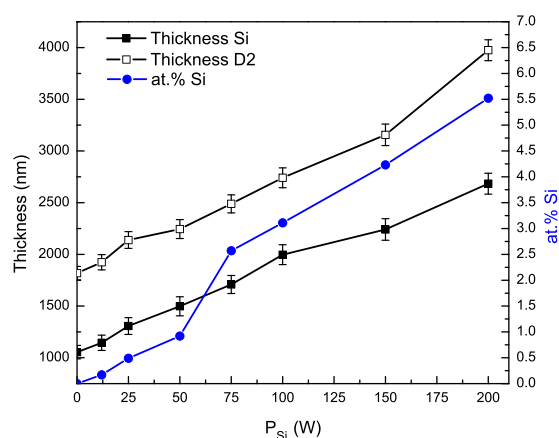

FIG. 2. (Color online) Thickness of the coatings vs the power applied to the Si target (P$_{Si}$) for samples deposited on both substrates; Si (45 min) and D2 steel (90 min). The right-axis presents the increase in the Si at. % as a function of the P$_{Si}$.

TABLE I. Deposition power applied to the Si target, Si atomic percentage, O/Nb atomic ratio, crystalline grain size obtained from the XRD data, and the hardness and Young's modulus obtained from the nanoindentation analysis.

Sample	Power (W)	Si at. %[a]	O/Nb[a]	Grain size (nm)	Hardness (GPa)[b]	Young's modulus (GPa)[a]
NBO$_X$	0	0	2.4 ± 0.1	40 ± 2	8.4 ± 0.7	134.5 ± 3.5
NBO$_X$-12	12	0.2 ± 0.1	2.4 ± 0.1	38 ± 2	11.1 ± 0.7	161.1 ± 4.7
NBOX-25	25	0.5 ± 0.1	2.5 ± 0.1	32 ± 2	12.7 ± 1.2	174.8 ± 2.3
NBOX-50	50	0.9 ± 0.1	2.5 ± 0.1	23 ± 2	17.6 ± 0.9	181.7 ± 4.2
NBO$_X$-75	75	2.6 ± 0.2	2.6 ± 0.1	21 ± 2	9.9 ± 0.8	149.2 ± 3.6
NBOX-100	100	3.1 ± 0.3	2.6 ± 0.1	—	7.7 ± 0.5	138.6 ± 4.3
NBOX-150	150	4.2 ± 0.2	2.7 ± 0.1	—	7.3 ± 0.7	134.8 ± 4.6
NBOX-200	200	5.5 ± 0.2	2.9 ± 0.1	—	6.2 ± 0.8	130.3 ± 2.7

[a]Mean ± standard deviation.
[b]Median ± standard error.

also bonding to silicon. Further experiments using x-ray photoelectron spectroscopy are required to confirm the respective bonding configurations.

The XRD patterns of the NbO$_x$:Si samples are reported in Fig. 3. For P$_{Si}$ values below 75 W, the diffraction peaks correspond to the T-Nb$_2$O$_5$, which is the orthorhombic phase (ICDD-01-071-0336). The sample without Si (NbO$_x$) and the NbO$_x$-P$_{Si}$ samples with P$_{Si}$ values below 50 W presents a preferential growth along the (200) direction. However, there is a change in the preferred orientation in the NbO$_x$-75 sample, where the (001) becomes the preferred plane. Above this power of 75 W, the coatings present broad diffraction peaks that indicate the formation of extremely small nanocrystallites or amorphous oxide despite an annealing

treatment at 550 °C performed on all of the samples. It is important to note that there are no diffraction peaks associated with Si, SiO$_2$, other Nb-O phases or Nb-Si phases[65] present in the patterns.

The grain sizes were estimated using the Halder–Wagner method[66] for the samples presenting clear diffraction peaks (Table I). The grain size is seen to decrease from 40 ± 2 nm in the NbO$_x$ coating to 21 ± 2 nm in the NbO$_x$-75 sample. The addition of Si into the NbO$_x$ coatings induces a progressive reduction of the grain sizes as the Si content is increased until a point that a nanocrystalline or amorphous state is obtained.

B. Optical properties

One property that has been reported to vary among the different Nb-O phases is the optical absorption. Specifically, NbO exhibits metallic behavior, NbO$_2$ is cataloged as a low band-gap semiconductor (optical band gap, E$_g$, between 0.5 and 1.2 eV have been reported) and the Nb$_2$O$_5$ and nonstoichiometric phases (phases between NbO$_2$ and Nb$_2$O$_5$) are considered high band-gap semiconductors (E$_g$ > 3.0 eV).[14] Therefore, we performed an analysis of the optical properties to determine the presence of noncrystalline phases that could not be observed by XRD. The ellipsometric spectra were measured in the 1.5–5 eV range for samples deposited on the Si and D2 steel substrates, and similar spectra were obtained. The ellipsometry data were analyzed using the Delta-Psi$^®$ software. The parametric function used to simulate the properties of the niobium oxide layer was the Tauc-Lorentz dispersion function,[67] shown in Eq. (1), which was appropriate because the XRD results indicated that the crystalline domain was nanocrystalline. Therefore,
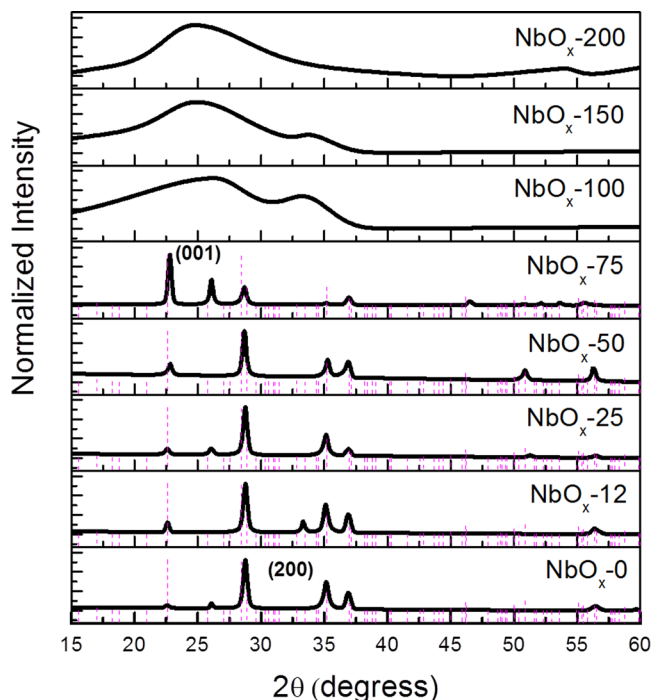

FIG. 3. (Color online) X-ray diffraction patterns of the NbO$_x$:Si samples after the annealing treatment at 550 °C for 2 h in air. The samples produced at P$_{Si}$ ≤ 75 W were crystalline and exhibit the T-Nb$_2$O$_5$ phase. The position and relative intensity of the diffraction peaks of the T-Nb$_2$O$_5$ (JCDPS card No. 01-071-0336) are also included as the dashed lines. The NbO$_x$-100 to NbO$_x$-200 coatings showed broad diffraction bands.

$$\varepsilon = \varepsilon_1 + i\varepsilon_2 \rightarrow \varepsilon_2 = \begin{cases} \dfrac{1}{E} \dfrac{AE_oC(E-E_g)^2}{\left(E^2 - E_o^2\right)^2 + C^2E^2}, & E > E_g \\ 0 & E \leq E_g \end{cases},$$

$$\varepsilon_1 \ \ Kramers - Kronig \ integral \qquad (1)$$

where E is the photon energy, E$_o$ is the oscillator energy, E$_g$ is the optical band gap, and A and C are parametric values.[67]

The first fittings were done using a single-homogeneous material and considering the optical properties of the Nb_2O_5 phase,[1] as suggested by the XRD data. However, no fitting was possible, and, as mentioned above, the visible-light transmittance was null for the samples with P_{Si} values lower than 100 W, and for $P_{Si} > 100$ W, it increased only slightly. This contradicts the expected results for a pure Nb_2O_5, which even in the amorphous[24] or nonstoichiometric state are transparent.[14] Therefore, a single-heterogeneous layer consisting of a mixture of the Nb_2O_5 and a secondary phase [NbO_y (y < 2.5)] was proposed, as exemplified in Fig. 4(a). The Bruggeman effective medium approximation[68] was

used, and the volume fraction was one of the fitting parameters. The ellipsometric parametric models used to consider the contribution from the different niobium oxide phases were proposed based on previous references,[1,69] and the Nb_2O_5 phase was modeled using the single Tauc-Lorentz oscillator with a resonance frequency around 5 eV and an optical band gap of about 3.5 eV. Meanwhile, the substoichiometric NbO_y (y < 2.5) phase was modeled using two Tauc-Lorentz oscillators and a smaller optical gap to consider the properties of the low band-gap NbO_2 or the metallic NbO phases. No phase corresponding to Si or SiO_x was included because no evidence of Si segregation was obtained with any of the other characterization techniques. Using this approach, it was possible to obtain good fittings of the ellipsometric spectra for all of the samples (except NbO_x-75), as shown in Fig. 4(b) for limited samples. In Fig. 4(b), the measured ellipsometric spectra ($I_S = \sin2\psi\sin\Delta$ and $I_C = \sin2\psi\cos\Delta$)[70] are represented by the symbols (some data points removed for clarity) and the continuous lines are the results of the fitting. Figure 4(c) shows the effective refractive index and extinction coefficient of the coatings estimated from the heterogeneous layer composed of Nb_2O_5 and the substoichiometric NbO_y component. These values are similar to those reported by other authors.[1,3] The optical band gap (E_g) obtained for the Nb_2O_5 phase ranges between 3.5 and 3.8 eV, while that for the substoichiometric phase is below 1.0 eV. Table II shows the relative fraction of both the Nb_2O_5 and the sub-stoichiometric NbO_y phases, including also the figure of merit (the lowest values are the best) from the fitting process of the samples deposited on Si. However, similar values ($\pm2\%$–5% variation) are obtained when the samples deposited on the D2 steel are modeled.

Therefore, it is important to note that it is possible to probe the presence of other Nb-O phases by performing the ellipsometric analysis and that the relative fraction of each phase is similar for all of the Si contents, i.e., $\sim70\%$–80% for the Nb_2O_5 and $\sim30\%$–20% for the substoichiometric NbO_y. As observed in Table I, the O/Nb ratio does not decrease with the Si content, which is in agreement with the fact that the fraction of the substoichiometric component remains approximately constant for all samples. Thus, the increase in the O/Nb ratio may be associated with the formation of SiO_x bonds, which is probable owing to the high enthalpy necessary for their formation.
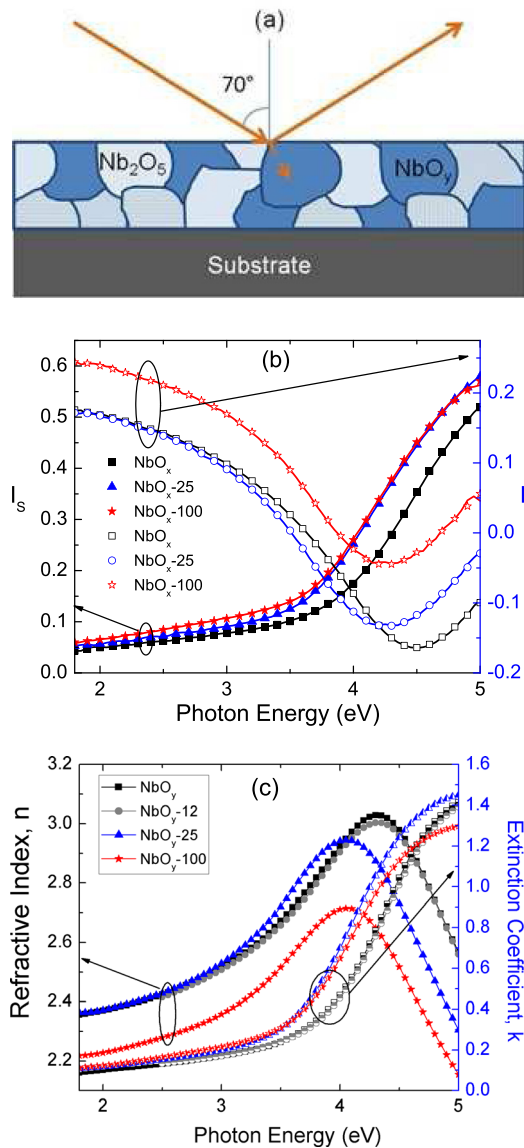
FIG. 4. (Color online) (a) Schematic of the effective medium model used to simulate the ellipsometric results. The model assumes the two phases of Nb_2O_5 and a substoichiometric amorphous NbO_y phase. (b) Examples of the fitting of the ellipsometric spectra showing good agreement between experimental data (symbols) and the model (continuous lines). For the configuration used by the phase modulated ellipsometer, $I_S = \sin2\psi\sin\Delta$ and $I_C = \sin2\psi\cos\Delta$ (c) The effective refractive index of the coatings estimated from the heterogeneous layer composed of Nb_2O_5 and the substoichiometric NbO_y component.

TABLE II. Volume percentage of each phase and the figure of merit for the ellipsometric fitting (χ).

Sample	χ^2	Nb_2O_5 (%)	NbO_y (%)
NBO_X	0.018	73.0 ± 0.5	27.0 ± 0.5
NBO_X-12	0.017	70.7 ± 0.3	29.3 ± 0.3
NBOX-25	0.023	71.4 ± 0.3	28.6 ± 0.3
NBOX-50	0.025	71.8 ± 0.4	28.2 ± 0.4
NBO_X-75	—	—	—
NBOX-100	0.053	71.9 ± 0.6	28.1 ± 0.6
NBOX-150	0.052	77.8 ± 0.7	22.2 ± 0.7
NBOX-200	0.087	74.4 ± 0.7	25.55 ± 0.7

C. Raman spectroscopy

Figure 5 shows representative micro-Raman spectra of some of the samples. The Raman spectra overlapped with a broad fluorescence band, which may be related to the low-band gap phase since the Raman excitation energy (2.41 eV) is larger than the optical band gap.[71] The fluorescence background may hide from view some low intensity signals, so only three peaks are observed and they are identified as corresponding to the Nb_2O_5 (Refs. 33 and 72) phase. The spectrum of NbO_2 contains other bands,[71] including one very intense band at $405\,cm^{-1}$, not observed in any of the samples. Independent of the Si content, there is a strong band around 500–$700\,cm^{-1}$ that is assigned to the symmetric stretching mode of the NbO_6 octahedra (S peak) and two additional bands in the 200–$300\,cm^{-1}$ region assigned to the bending modes of the Nb-O-Nb linkages (B_1 and B_2 peaks). The fact that all samples present similar spectra indicates that the same Nb-O-Nb structure is preserved locally. Similar to the XRD results, micro-Raman analyses performed on different positions within the same sample do not show the presence of other Nb-O or Si-associated phases. On the other hand, analysis of the peak positions and relative intensities indicate that some variations in the bonding characteristics occurred as a result of the Si incorporation. Figures 6(a)–6(c) show the peak position as a function of the P_{Si}, wherein the center peak position is obtained by adjusting the Gaussian functions at the two wave-number regions. The main peak (stretching Nb-O-Nb mode, S peak) is seen to shift from $685\,cm^{-1}$ for the NbO_x sample to about $675\,cm^{-1}$ as the Si content increases. Small ($3.4\,cm^{-1}$) red-shifts in

this signal have been previously associated with phase transformations, as, for example, from the $TT\text{-}Nb_2O_5$ to the $T\text{-}Nb_2O_5$ phase,[33] but no phase change is observed as the Si content increases and the S peak shift is much larger. This larger decrease in the wave-number ($\sim10\,cm^{-1}$) of the S peak is probably owing to a decrease in the bond order of the niobia polyhedral,[72] which is also confirmed by the increase in the width of the S peak [Fig. 6(e)]. Both changes are an indication that the structure becomes more disordered as the Si content is increased. Figures 6(c) and 6(d) show the relative intensity of the bending modes normalized to the stretching mode, wherein the B_1 peak intensity increases while the B_2 peak intensity decreases and the distinction between the two bending modes decreases as the disorder increases. Nevertheless, it is significant to note that the amorphous as-deposited NbO_x and NbO_x:Si samples do not exhibit any Raman signal. The presence of the Raman signal in the $NbO_x\text{-}P_{Si}$ samples ($P_{Si} > 75\,W$) suggests that the Si addition induces a decrease in the grain size (no longer measurable by XRD), but not the complete amorphization of the samples.

D. Topography and mechanical properties

Figures 7(a)–7(d) show the surface morphology of the coatings using SEM images of some samples, where no significant differences can be observed among the samples. Similar cauliflower-like features are observed for both the crystalline and amorphous samples. Nonetheless, the root mean square roughness value estimated using profilometry shows a small reduction from $40.16 \pm 2.89\,nm$ for the NbO_x sample to $26.34 \pm 1.92\,nm$ for the amorphous $NbO_x\text{-}200$ sample. These roughness values did not have significant effect on the scattering of light since they are lower than the wavelengths used.

After the determination of the structural variations of the NbO_x:Si samples, the mechanical–tribological properties were measured. The hardness and Young's modulus were obtained from nanoindentation measurements that provide information on the mechanical properties of the materials through modeling of the indenter load–displacement curves. In general, the load–displacement curve is influenced by the properties of the coating and the substrate. In this work, we used indentation loads wherein the penetration depth was less than 10% of the coating thickness to obtain only the hardness of the coatings.[62] Figure 8 shows the hardness and elastic modulus of the different NbO_x:Si samples as a function of the power applied to the Si target, P_{Si}. The nanoindentation experiments are done for both the Si and D2 steel substrates, and both data are presented in Fig. 8. There is a larger influence from the substrate mechanical properties upon the determination of the elastic modulus because it influences the elastic response even at low loads.[62] It can be seen that the hardness of the NbO_x sample (on D2) is $8.41 \pm 0.72\,GPa$, which is similar to the values reported by Mazur *et al.*[2] for $T\text{-}Nb_2O_5$. As the Si content is increased, the hardness increases up to $17.62 \pm 0.89\,GPa$ for the $NbO_x\text{-}50$ sample to nearly double its original value. However,
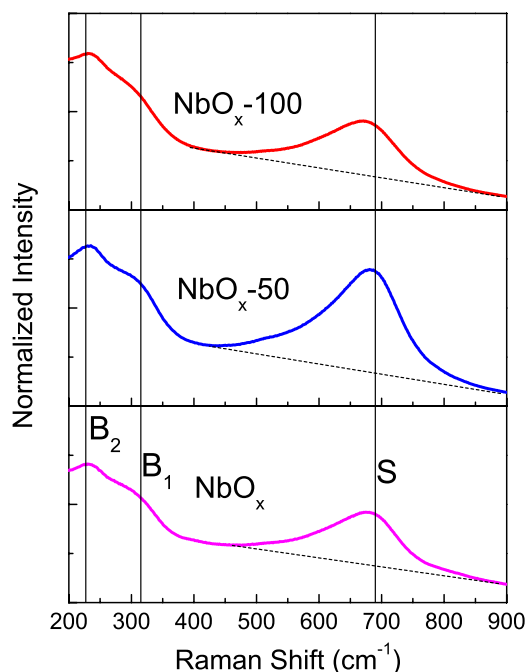
FIG. 5. (Color online) Micro-Raman spectra of the samples NbO_x:Si samples; all of the annealed (amorphous or crystalline) samples presented similar spectra, so only three of them are shown. The three characteristics bands observed for all films were identified as S, B_1 and B_2 and are related to the modes of $T\text{-}Nb_2O_5$ phase.
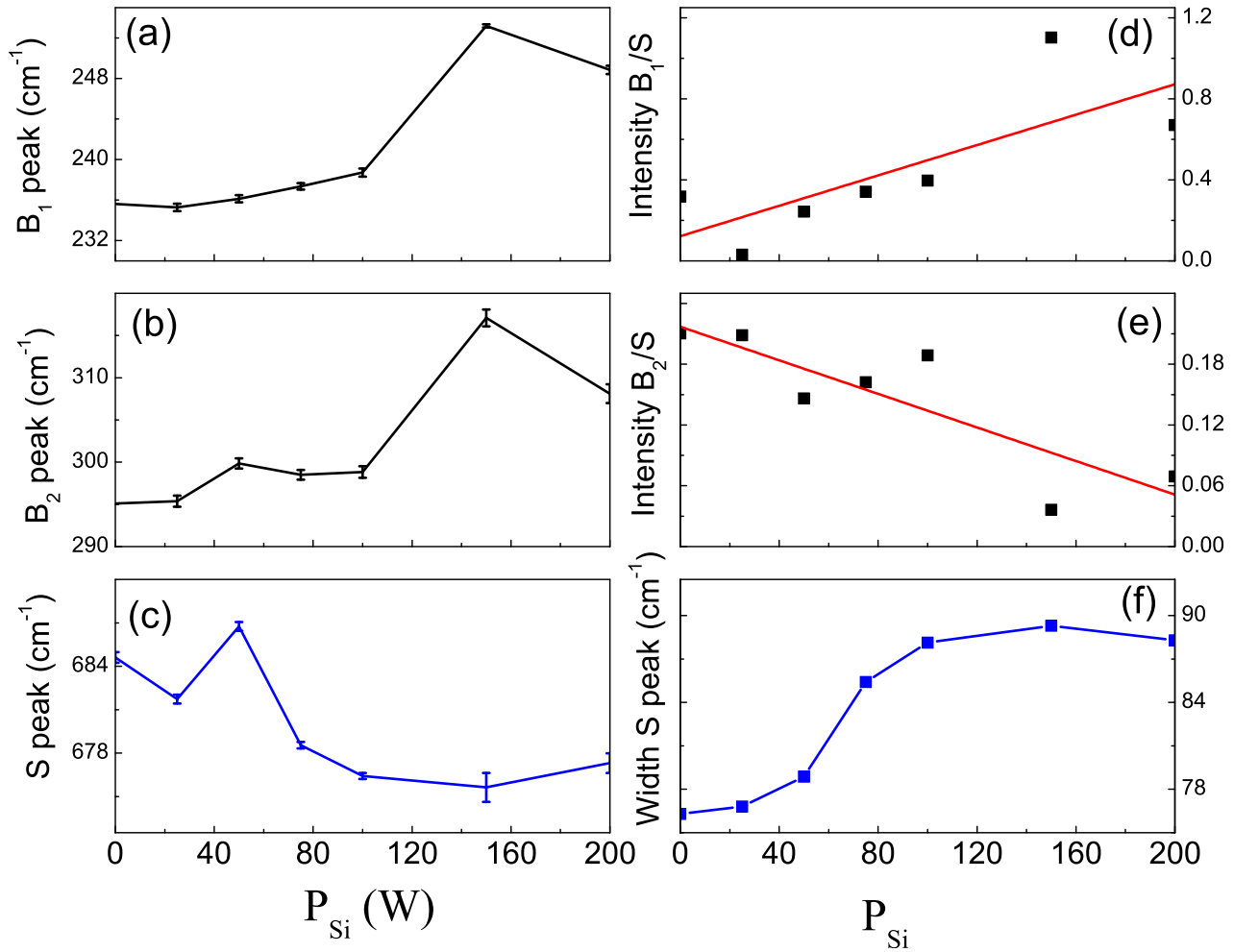
FIG. 6. (Color online) Variations of the Raman spectra as a function of Si incorporation (or the P$_{Si}$). The position shifts of the (a) S, (b) B$_1$, and (c) B$_2$ peaks, and the relative intensities of the (d) B$_1$/S and (d) B$_2$/S peaks. (e) The width of the main S peak corresponding to the stretching mode.

further increase in the Si content leads to a hardness decrease to 6.23 ± 0.82 GPa for the NbO$_x$-200 sample, which is lower than the hardness of the T-Nb$_2$O$_5$ sample and is closer to the hardness of SiO$_2$ coatings [reported about 5–6.5 GPa (Ref.
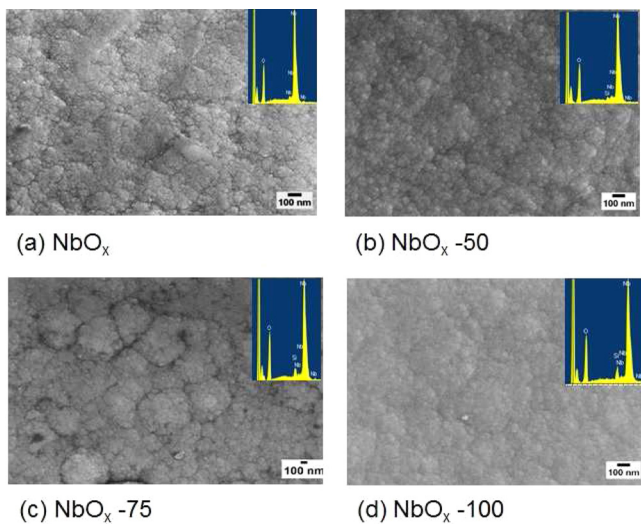

FIG. 7. (Color online) Surface morphology of the samples does not show strong variations as a function of the P$_{Si}$. Representative SEM micrographs of the surfaces of: (a) NbO$_x$, (b) NbO$_x$-50, (c) NbO$_x$-75, (d) NbO$_x$-100 exhibiting and morphology shows an amorphous nature. (Insets) Corresponding EDS analysis where Si is clearly observed.
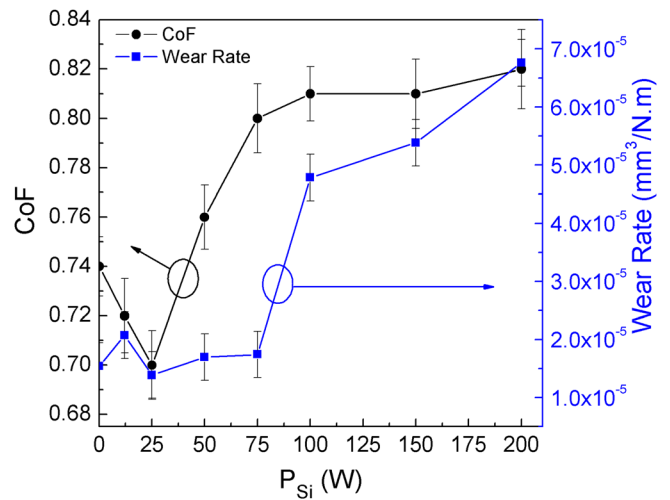

FIG. 8. (Color online) Results of the nanoindentation analysis, plotting the hardness and elastic moduli of the samples as a function of the power applied to the Si substrate for both the Si and D2 steel substrates.

73)]. The elastic modulus, also shown in Fig. 8, presents a similar trend as that of the hardness. The elastic modulus values vary from 134.50 ± 3.54 GPa for NbO_x to 181.65 ± 4.21 GPa for NbO_x-50 and finally decrease to 114.34 ± 2.54 GPa for NbO_x-200.

Prior to the measurements of the coefficient of friction (CoF), the scratch test was used to determine the critical load that the samples could support before the first failure event occurs.[74] Figure 9 shows examples of the scratch images, where the adhesive failure load at which the coating detaches from the substrate is indicated. Only the NbOx-100 sample fails by compressive spallation at very low loads (<20 N). The mechanism of the failure of the other samples changes randomly from buckling/spallation to films that only present plastic deformation. Therefore, as described by Bull,[75] we have not tried to correlate the critical loads to the Si incorporation or to the structure. The important message is that the coatings do not fail at the loads used for nanoin- dentation or CoF measurements. Finally, the variation of the CoF and the wear-rate volume as a function of the P_{Si} are presented in Fig. 10. The CoF shows a small dip for sample NbO_x-25 with the lowest value of 0.70, which rapidly increases for the other samples and reaches a CoF of 0.81. On the other hand, the wear-rate remains similar for all of the crystalline samples (NbO_x to NbO_x-75) and shows an increase of more than twice the value as the Si content increases and the samples become amorphous. The trend in both figures of the CoF and wear-rate is similar, and their error bars suggest that there are small and statistically signif- icant variations in both parameters, but such minute varia- tions have no implications for real applications.
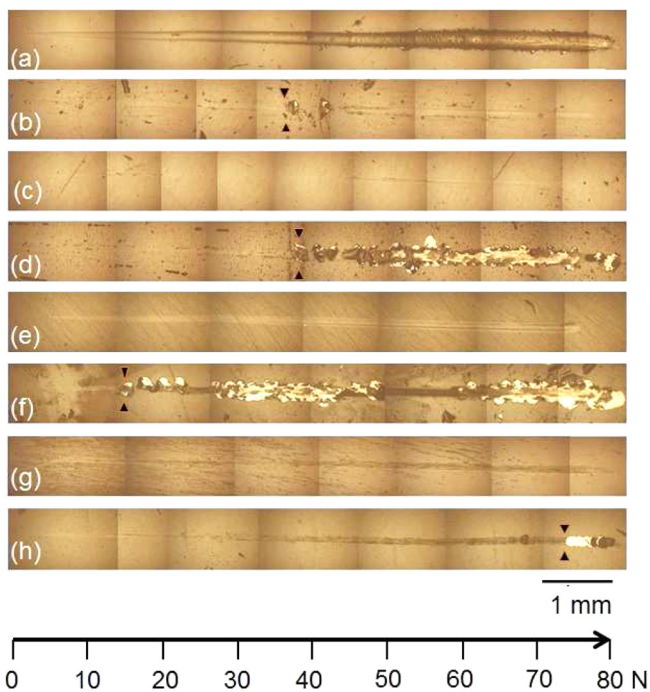

FIG. 9. (Color online) Micrograph of the full scratch of the NbO$_x$:Si coatings deposited on the D2 steel substrate with a bonding Nb layer. The triangles indicate the first adhesive failure event.
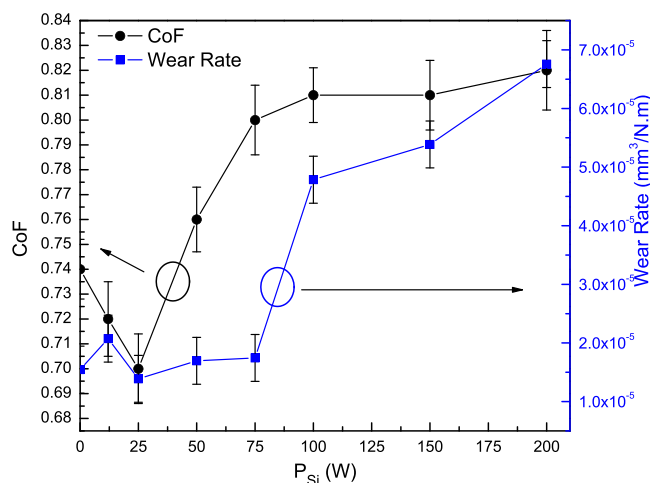
FIG. 10. (Color online) Results of the pin-on-disk analysis showing the vari- ation of the coefficient of friction and the wear-rate as a function of the P_{Si}.

E. Discussion

The objective of the present work was to evaluate the effect of Si addition into the structure and properties of nio- bium oxide coatings. Therefore, a series of NbO$_x$:Si coatings were produced by cosputtering from independent targets of Nb and Si. The as-deposited coatings were amorphous, and all the films were therefore annealed at 550 °C for 2 h in air. After annealing, XRD measurements indicated that the T-Nb₂O₅ structure was obtained. This was in good agree- ment with previous reports that indicated that at such a tem- perature range the orthorhombic phase should be obtained. However, by analyzing the optical properties and the XRD data of the coatings, it was evident that an amorphous NbO$_y$ ($y < 2.5$) phase was also present. This NbO$_y$ component explains the low optical transmittance of the samples, but the fraction of this component was not dependent upon the Si content. Therefore, it is reasonable to say that the struc- tural modifications of the samples were owing to the incor- poration of silicon. For example, when considering the decrease in the grain size and the subsequent increase in the hardness (Fig. 8), it was found that the grain size of the NbO$_x$:Si coatings ($P_{Si} < 50$ W) decreased from 40 to 23 nm and the nanohardness increased from 8.7 to 17.6 GPa. The Si at. % estimations were done using the EDS of coatings de- posited on D2 steel. The values obtained below 1 at. % might not be very accurate owing to the low resolution of the EDS, but the incorporation of Si was clearly identified (see the inset in Fig. 7). The XRD analysis showed that, for these samples, the structure was the orthorhombic T-Nb₂O₅ phase with a preferred (200) crystalline orientation. The Halder–Wagner method was used to calculate the crystalline domain (grain size), which allowed the separation of the effect of both the finite size and the strain upon the peak broadening, and the results indicated that no significant strain was introduced because of the Si addition. This can be observed in Fig. 3 where no significant peak shifts are observed, which may be owing to stress relief during the 2 h thermal treatment at 550 °C. Therefore, we can conclude that the hardening is not owing to an increase in the strain.

However, the absence XRD-peak shifts is also an indication that Si was not incorporated either substitutionally or interstically into the T-Nb$_2$O$_5$ structure. More likely, the Si was allocated into the grain boundaries, as has been observed in other similar works,[50–54] or was substituionally incorporated into the NbO$_y$ substoichiometric component. Moreover, the allocation of Si into the grain boundaries could also explain the reduction in the Nb$_2$O$_5$ grain size as a function of the addition of Si atoms. Actually, the reduction in the crystalline domain continued gradually as the Si content increased, reaching 21 nm for the NbO$_x$-75 sample and values not measureable by XRD for the last three samples (up to 5.5 Si at. %). We also observed a variation in the preferred orientation for the Nb$_2$O$_5$-75 sample from the (200) to the (001). Variations in the preferred orientation have also been reported for metal nitrides when Si is incorporated,[55,76,77] or as a consequence of an increase in the energy during the deposition.[78] In the case of the Nb$_2$O$_5$-75 sample, the grain size was smaller than that of the Nb$_2$O$_5$-50 samples, but the hardness did not exhibit the increasing trend, but had already begun to reduce (9.9 GPa), probably owing to the change in the preferred orientation.

It is well known that the hardness and elastic modulus of polycrystalline materials can be improved through grain size refinement or the Hall-Petch effect,[79,80] where the relationship between the hardness and the grain size is given by

$$H = H_o + k_h d^{\frac{-1}{2}}, \tag{2}$$

where H is the hardness of the material, d is the grain size, and the H_o and k_h are constants related to the material.[79,80] Nonetheless, it has been shown by Chokshi *et al.*[81] that the Hall–Petch effect is valid up to a minimum grain size of about 10–20 nm, and that a further decrease in grain size will lead to a decrease in the hardness (Inverse Hall–Petch effect).

Figure 11 plots the graphic representation of Eq. (2) showing the hardness versus the square root of the inverse of
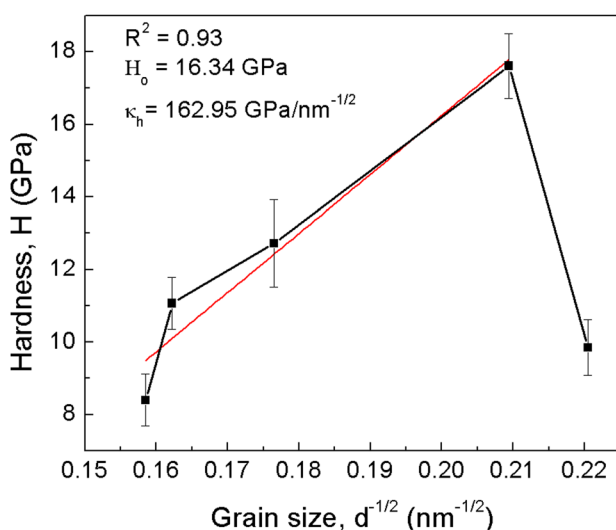

FIG. 11. (Color online) Hardness vs square root of the inverse of the crystalline grain size (i.e., Hall–Petch relationship).

the grain size. For the Nb$_2$O$_5$-Si samples with P$_{Si}$ below 50 W, wherein hardness enhancement was observed, a relatively good linear fit could be obtained (R = 0.93). This linear fit explains the mechanism through which the addition of small amounts of Si induced a hardness enhancement in the NbO$_x$ samples. However, the sudden decrease with further Si addition is not so clear. First, for the NbO$_x$-75 sample, there is a change in the preferred orientation whereupon even a smaller grain size presents lower hardness. This may be the consequence of the anisotropy in the intrinsic elastic modulus, as has been observed for metal nitrides.[82] For the other samples, however, it is not clear if the hardness decrease is owing to an inverse-Hall–Petch effect (because grain size could not be estimated from the XRD data), or to the growth of the interfacial Si-rich phase situated in the grain boundary, or to a decrease in the density of the film owing to the amorphization. The metal nitride–Si nanocomposite coatings also presented a decrease in the hardness for Si contents above 10–12 at. % (depending upon the system and deposition method), which has been explained as a consequence of the growth of the interfacial a-SiN$_x$ layer beyond one monolayer. However, in the present case, we do not yet have evidence of the formation of a nanocomposite structure, but simply have the macrostructural evidence that suggests that Si was segregated into the grain boundaries of the Nb$_2$O$_5$ crystals to limit their growth. This is in agreement with the Raman results that suggest that the predominant local bonding remained as NbO$_x$ polyhedra without the evidence of the formation of Si-based structures. On the other hand, the relative fraction of the substoichiometric NbO$_y$ component, as determined from optical analysis, remained similar between the crystalline (P$_{Si} \leq 75$ W) and the amorphous samples (P$_{Si} > 75$ W). Therefore, its contribution to the structural, mechanical, and tribological properties is relevant but does not vary with the Si addition. Interestingly, small additions of Si led to a small but significant increase in the coating–substrate adhesion and a reduction in both the friction coefficient and wear-rate. We did not find any previous communication reporting the tribological performance of niobium oxide layers, so the values obtained herein cannot be compared. Oxide surfaces are important for tribological applications because it has been observed that, during dry machining or high-temperature sliding bearing applications of metallic components, a low-friction layer is formed. These are known as lubricious oxides[83] (MoO$_3$, V$_2$O$_5$, WO$_3$, Re$_2$O$_7$, PdO, FeO, Co$_2$O$_3$, SnO$_2$, Cr$_2$O$_3$, ZnO) and, for some applications, metallic elements are added to the alloy or the coating to induce the formation of this self-lubricating oxide surface.[84,85] Two explanations for the low CoF of some oxide layers have been proposed. Erdemir[86] has proposed a chemical approach that relates the CoF with the ionic potential whereby the ratio of the cationic charge is related to the radius of the cation. There is not a clear boundary in this approach, but larger ionic potentials correspond to lower CoF values at elevated temperatures. Prakash and Celis[83] have improved this model by also considering the CoF of the oxide layers in a wider range of temperatures and conclude that a better approach is to correlate the CoF with the

polarizability of the ions. Both papers collected CoF values of a wide variety of oxides from the literature, but none of them included any of the niobium oxides phases. The ionic potential of the Nb$_2$O$_5$ (7.4) is high enough to expect a low CoF at elevated temperatures according to Erdemir.[86] However, according to the polarizability model,[83] no NbO$_x$ phases are considered of interest to achieve low friction and wear.

In summary, we have observed that it is possible to enhance the mechanical properties of the niobium oxide coatings through the incorporation of a small percentage of silicon. However, to take full advantage of this effect, a pure Nb$_2$O$_5$ phase should be obtained, whereupon the method proposed could be used to produce hard and wear-resistant transparent coatings. Moreover, to fully understand the role played by the addition of Si upon the structural changes, nanoscale and local-bonding characterization are required.

IV. SUMMARY AND CONCLUSIONS

Silicon-containing niobium oxide coatings were deposited by cosputtering, whereupon a significant increase was found in the hardness (from 8.4 to 17.6 GPa) when small fractions of Si were added, and the grain size was reduced from 40 to 23 nm. The predominant structure of the films was ortho-rhombic T-Nb$_2$O$_5$ but a ~30% volume fraction of a substoichiometric and amorphous NbO$_y$ component was found for all films. There was no evidence of Si or Si-based segregated particles based upon the macroscopic evaluation via XRD, SEM, and Raman. The hardness enhancement was associated with the grain size reduction following a Hall–Petch relation. This grain size reduction was probably owing to the allocation of Si at the grain boundaries that limited the growth of the Nb$_2$O$_5$ crystalline domains, which eventually led to an XRD-amorphous phase.

ACKNOWLEDGMENTS

[1]M. Serényi, T. Lohner, P. Petrik, Z. Zolnai, Z. E. Horváth, and N. Q. Khánh, Thin Solid Films **516**, 8096 (2008).
[2]M. Mazur, M. Szymanska, D. Kaczmarek, M. Kalisz, D. Wojcieszak, J. Domaradzki, and F. Placido, Appl. Surf. Sci. **301**, 63 (2014).
[3]H. Szymanowski, O. Zabeida, J. E. Klemberg-Sapieha, and L. Martinu, J. Vac. Sci. Technol., A **23**, 241 (2005).
[4]T. Tamai, M. Haneda, T. Fujitani, and H. Hamada, Catal. Commun. **8**, 885 (2007).
[5]A. G. S. Prado, L. B. Bolzon, C. P. Pedroso, A. O. Moura, and L. L. Costa, Appl. Catal., B **82**, 219 (2008).
[6]I. Nowak and M. Ziolek, Chem. Rev. **99**, 3603 (1999).
[7]M.-R. Ok, R. Ghosh, M. K. Brennaman, R. Lopez, T. J. Meyer, and E. T. Samulski, ACS Appl. Mater. Interfaces **5**, 3469 (2013).
[8]R. Ghosh, M. K. Brennaman, T. Uher, M.-R. Ok, E. T. Samulski, L. E. McNeil, T. J. Meyer, and R. Lopez, ACS Appl. Mater. Interfaces **3**, 3929 (2011).
[9]M. Qamar, M. Abdalwadoud, M. I. Ahmed, A. M. Azad, B. Merzougui, S. Bukola, Z. H. Yamani, and M. N. Siddiqui, ACS Appl. Mater. Interfaces **7**, 17954 (2015).
[10]M. A. Aegerter, Sol. Energy Mater. Sol. Cells **68**, 401 (2001).
[11]U. Cvelbar and M. Mozetic, J. Phys. D: Appl. Phys. **40**, 2300 (2007).
[12]Ö. D. Coşkun, S. Demirel, and G. Atak, J. Alloys Compd. **648**, 994 (2015).
[13]S. M. Mirvakili, M. N. Mirvakili, P. Englezos, J. D. W. Madden, and I. W. Hunter, ACS Appl. Mater. Interfaces **7**, 13882 (2015).
[14]C. Nico, T. Monteiro, and M. P. F. Graça, Prog. Mater. Sci. **80**, 1 (2016).
[15]S. Clima *et al.*, J. Electrochem. Soc. **157**, G20 (2010).
[16]H. Zillgen, M. Stenzel, and W. Lohwasser, Act. Passive Electron. Compon. **25**, 147 (2002).
[17]T. Hyodo, J. Ohoka, Y. Shimizu, and M. Egashira, Sens. Actuators, B **117**, 359 (2006).
[18]R. Ab Kadir, R. A. Rani, M. M. Y. A. Alsaif, J. Z. Ou, W. Wlodarski, A. P. O'Mullane, and K. Kalantar-zadeh, ACS Appl. Mater. Interfaces **7**, 4751 (2015).
[19]H. Wylezich, H. Mähne, J. Rensberg, C. Ronning, P. Zahn, S. Slesazeck, and T. Mikolajick, ACS Appl. Mater. Interfaces **6**, 17474 (2014).
[20]E. Eisenbarth, D. Velten, M. Muller, R. Thull, and J. Breme, J. Biomed. Mater. Res., Part A **79A**, 166 (2006).
[21]P. N. Rojas and S. E. Rodil, Int. J. Electrochem. Sci. **7**, 1443 (2012).
[22]S. Nagarajan, V. Raman, and N. Rajendran, Mater. Chem. Phys. **119**, 363 (2010).
[23]M. F. Pillis, G. A. Geribola, G. Scheidt, E. G. de Araújo, M. C. L. de Oliveira, and R. A. Antunes, Corros. Sci. **102**, 317 (2016).
[24]G. Ramirez, S. E. Rodil, S. Muhl, D. Turcio-Ortega, J. J. Olaya, M. Rivera, E. Camps, and L. Escobar-Alarcon, J. Non-Cryst. Solids **356**, 2714 (2010).
[25]E. Çetinörgü-Goldenberg, J. E. Klemberg-Sapieha, and L. Martinu, Appl. Opt. **51**, 6498 (2012).
[26]H. Schafer, R. Gruehn, and F. Schulte, Angew. Chem. Int. Ed. **5**, 40 (1966).
[27]K. Naito, N. Kamegashira, and N. Sasaki, J. Solid State Chem. **35**, 305 (1980).
[28]J. A. Roberson and R. A. Rapp, J. Phys. Chem. Solids **30**, 1119 (1969).
[29]S. Kimura, J. Solid State Chem. **6**, 438 (1973).
[30]R. A. Rani, A. S. Zoolfakar, A. P. O'Mullane, M. W. Austin, and K. Kalantar-Zadeh, J. Mater. Chem. A **2**, 15683 (2014).
[31]A. Le Viet, R. Jose, M. V. Reddy, B. V. R. Chowdari, and S. Ramakrishna, J. Phys. Chem. C **114**, 21795 (2010).
[32]L. A. Reznichenko, V. V. Akhnazarova, L. A. Shilkina, O. N. Razumovskaya, and S. I. Dudkina, Crystallogr. Rep. **54**, 483 (2009).
[33]L. K. S. Herval, D. von Dreifus, A. C. Rabelo, A. D. Rodrigues, E. C. Pereira, Y. G. Gobato, A. J. A. de Oliveira, and M. P. F. de Godoy, J. Alloys Compd. **653**, 358 (2015).
[34]R. L. Karlinsey, Electrochem. Commun. **7**, 1190 (2005).
[35]I. Sieber, H. Hildebrand, A. Friedrich, and P. Schmuki, Electrochem. Commun. **7**, 97 (2005).
[36]J. Choi, J. H. Lim, J. Lee, and K. J. Kim, Nanotechnology **18**, 055603 (2007).
[37]I. Komatsu, H. Aoki, M. Ebisawa, A. Kuroda, K. Kuroda, and S. Maeda, Thin Solid Films **603**, 180 (2016).
[38]M. Schmitt and M. A. Aegerter, Electrochim. Acta **46**, 2105 (2001).
[39]N. Ozer, M. D. Rubin, and C. M. Lampert, Sol. Energy Mater. Sol. Cells **40**, 285 (1996).
[40]P. S. Patil, A. R. Patil, S. H. Mujawar, and S. B. Sadale, J. Mater. Sci. **16**, 35 (2005).
[41]S. Mujawar, A. Inamdar, C. Betty, V. Ganesan, and P. Patil, Electrochim. Acta **52**, 4899 (2007).
[42]M. T. Duffy, C. C. Wang, A. Waxman, and Kh. Zaininge, J. Electrochem. Soc. **116**, 234 (1969).
[43]J. Van Glabbeek and R. Van De Leest, Thin Solid Films **201**, 137 (1991).
[44]X. Xiao, G. Dong, C. Xu, H. He, H. Qi, Z. Fan, and J. Shao, Appl. Surf. Sci. **255**, 2192 (2008).
[45]K. Yoshimura, T. Miki, S. Iwama, and S. Tanemura, Jpn. J. Appl. Phys., Part 2 **34**, L1293 (1995).
[46]B. Hunsche, M. Vergohl, H. Neuhauser, F. Klose, B. Szyszka, and T. Matthee, Thin Solid Films **392**, 184 (2001).
[47]A. Foroughi-Abari and K. C. Cadien, Thin Solid Films **519**, 3068 (2011).
[48]N. Usha, R. Sivakumar, C. Sanjeeviraja, and M. Arivanandhan, Optik **126**, 1945 (2015).

[49]S. Venkataraj, R. Drese, C. Liesch, O. Kappertz, R. Jayavel, and M. Wuttig, J. Appl. Phys. **91**, 4863 (2002).

[50]S. Veprek, A. Niederhofer, K. Moto, T. Bolom, H. D. Mannling, P. Nesladek, G. Dollinger, and A. Bergmaier, Surf. Coat. Technol. **133**, 152 (2000).

[51]R. F. Zhang and S. Veprek, Phys. Rev. B **76**, 174105 (2007).

[52]U. W. Blass, T. Barsukova, M. R. Schwarz, A. Kohler, C. Schimpf, I. A. Petrusha, U. Muhle, D. Rafaja, and E. Kroke, J. Eur. Ceram. Soc. **35**, 2733 (2015).

[53]P. Karvankova, H. D. Mannling, C. Eggs, and S. Veprek, Surf. Coat. Technol. **146**, 280 (2001).

[54]D. Bernoulli, U. Muller, M. Schwarzenberger, R. Hauert, and R. Spolenak, Thin Solid Films **548**, 157 (2013).

[55]M. Benkahoul, C. S. Sandu, N. Tabet, M. Parlinska-Wojtan, A. Karimi, and F. Lévy, Surf. Coat. Technol. **188–189**, 435 (2004).

[56]E. Martinez, R. Sanjinés, O. Banakh, and F. Lévy, Thin Solid Films **447–448**, 332 (2004).

[57]M. Nose, W. A. Chiou, M. Zhou, T. Mae, and M. Meshii, J. Vac. Sci. Technol., A **20**, 823 (2002).

[58]A. A. Voevodin, A. L. Yerokhin, V. V. Lyubimov, M. S. Donley, and J. S. Zabinski, Surf. Coat. Technol. **86–87**, 516 (1996).

[59]C.-J. Tang, G. A. Porter, C.-C. Jaing, and F.-M. Tsai, Appl. Opt. **54**, 959 (2015).

[60]F. Richter, H. Kupfer, P. Schlott, T. Gessner, and C. Kaufmann, Thin Solid Films **389**, 278 (2001).

[61]R. Leitel, O. Stenzel, S. Wilbrandt, D. Gäbler, V. Janicki, and N. Kaiser, Thin Solid Films **497**, 135 (2006).

[62]S. J. Bull, J. Phys. D: Appl. Phys. **38**, R393 (2005).

[63]W. C. Oliver and G. M. Pharr, J. Mater. Res. **7**, 1564 (1992).

[64]A.C-05(2015), *Standard Test Method for Adhesion Strength and Mechanical Failure Modes of Ceramic Coatings by Quantitative Single Point Scratch Testing* (ASTM International, West Conshohocken, PA, 2007).

[65]T. P. Chow, K. Hamzeh, and A. J. Steckl, J. Appl. Phys. **54**, 2716 (1983).

[66]N. C. Halder and C. N. J. Wagner, Acta Crystallogr. **20**, 312 (1966).

[67]G. E. Jellison and F. A. Modine, Appl. Phys. Lett. **69**, 371 (1996).

[68]S. Bosch, J. Ferré-Borrull, N. Leinfellner, and A. Canillas, Surf. Sci. **453**, 9 (2000).

[69]A. Hara, T. N. Nunley, A. B. Posadas, S. Zollner, and A. A. Demkov, J. Appl. Phys. **116**, 213705 (2014).

[70]H. Fujiwara, *Spectroscopic Ellipsometry* (John Wiley & Sons, Ltd, 2007), p. 81.

[71]Z. Ye, Z. Zhengjun, and L. Yuanhua, J. Phys. D: Appl. Phys. **37**, 3392 (2004).

[72]J. M. Jehng and I. E. Wachs, Chem. Mater. **3**, 100 (1991).

[73]M. Cabibbo, D. Ciccarelli, and S. Spigarelli, Phys. Procedia **40**, 100 (2013).

[74]S. J. Bull, Surf. Coat. Technol. **50**, 25 (1991).

[75]S. J. Bull, Tribol. Int. **30**, 491 (1997).

[76]D. Oezer, G. Ramírez, S. E. Rodil, and R. Sanjinés, J. Appl. Phys. **112**, 114302 (2012).

[77]G. Ramírez, D. Oezer, M. Rivera, S. E. Rodil, and R. Sanjinés, Thin Solid Films **558**, 104 (2014).

[78]J. J. Olaya, S. E. Rodil, and S. Muhl, Thin Solid Films **516**, 8319 (2008).

[79]E. O. Hall, Proc. Phys. Soc. London, Sect. B **64**, 747 (1951).

[80]N. J. Petch, J. Iron Steel Inst. **174**, 25 (1953).

[81]A. H. Chokshi, A. Rosen, J. Karch, and H. Gleiter, Scr. Metall. **23**, 1679 (1989).

[82]D. Holec, M. Friák, J. Neugebauer, and P. H. Mayrhofer, Phys. Rev. B **85**, 064101 (2012).

[83]B. Prakash and J. P. Celis, Tribol. Lett. **27**, 105 (2007).

[84]N. Fateh, G. A. Fontalvo, G. Gassner, and C. Mitterer, Tribol. Lett. **28**, 1 (2007).

[85]W. Gulbiński, T. Suszko, W. Sienicki, and B. Warcholiński, Wear **254**, 129 (2003).

[86]A. Erdemir, Surf. Coat. Technol. **200**, 1792 (2005).